JACS
JOURNAL OF THE AMERICAN CHEMICAL SOCIETY
Article
pubs.acs.org/JACS

Through-Bond versus Through-Space Coupling in Mixed-Valence Molecules: Observation of Electron Localization at the Single-Molecule Scale

Rebecca C. Quardokus,[†] Yuhui Lu,[‡] Natalie A. Wasio,[†] Craig S. Lent,[‡] Frederic Justaud,[§] Claude Lapinte,[§] and S. Alex Kandel*,[†]

[†]Department of Chemistry and Biochemistry, University of Notre Dame, Notre Dame, Indiana 46556, United States
[‡]Department of Engineering, University of Notre Dame, Notre Dame, Indiana 46556, United States
[§]Sciences Chimiques de Rennes, UMR 6226 CNRS−Université de Rennes I, 35042 Rennes Cedex, France

ABSTRACT: Scanning tunneling microscopy (STM) is used to study two dinuclear organometallic molecules, *meta*-Fe2 and *para*-Fe2, which have identical molecular formulas but differ in the geometry in which the metal centers are linked through a central phenyl ring. Both molecules show symmetric electron density when imaged with STM under ultrahigh-vacuum conditions at 77 K. Chemical oxidation of these molecules results in mixed-valence species, and STM images of mixed-valence *meta*-Fe2 show pronounced asymmetry in electronic state density, despite the structural symmetry of the molecule. In contrast, images of mixed-valence *para*-Fe2 show that the electronic state density remains symmetric. Images are compared to constrained density functional (CDFT) calculations and are consistent with full localization of charge for *meta*-Fe2 on to a single metal center, as compared with charge delocalization over both metal centers for *para*-Fe2. The conclusion is that electronic coupling between the two metal centers occurs through the bonds of the organic linker, and through-space coupling is less important. In addition, the observation that mixed-valence *para*-Fe2 is delocalized shows that electron localization in *meta*-Fe2 is not determined by interactions with the Au(111) substrate or the position of neighboring solvent molecules or counterion species.

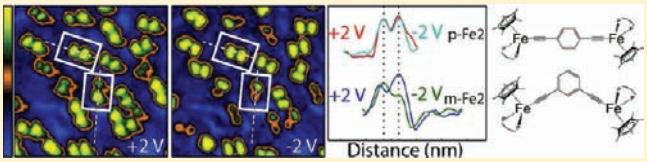

Experimental scanning tunneling microscopy (STM) results and theoretical calculations are presented in this article for two homodinuclear molecules, referred to as *meta*-Fe2 and *para*-Fe2 and shown in Figure 1. Each molecule is composed of two copies of the same Cp*Fe(dppe), metal−ligand unit, bound symmetrically about a central benzene ring with an ethynyl linker; the two molecules differ in their substitution pattern on this ring. We study these as neutral molecules, where each iron atom is in the +2 oxidation state, and as mixed-valence cations, where removal of a single electron results in +2/+ 3 oxidation states for the iron centers.[1−4]

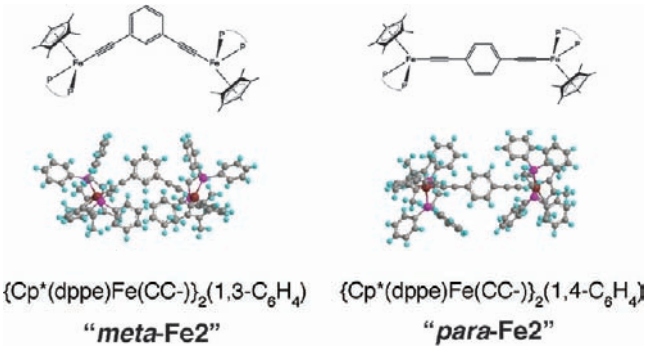

Figure 1. Dinuclear organometallic molecules, *meta*-Fe2 and *para*-Fe2.

By definition, mixed-valence molecules have two degenerate or nearly degenerate ground electronic states; for Fe2, these correspond to +2/+3 and +3/+2 oxidation states or superpositions thereof. The spatial distribution of electric charge will therefore depend heavily on the electronic coupling between the metal centers and the presence of perturbations in the molecular environment: weak coupling will allow even a modest perturbation to localize charge to one metal center, while strong coupling will likely result in electron delocalization unless a strong perturbation is present. By studying these molecules via a single-molecule technique, in ultrahigh vacuum, and with a relative absence of solvent, we hope to investigate the fundamentals of how molecular environment results in localization or delocalization of charge.

STM is well established as a technique for studying the conformation and electronic properties of single molecules adsorbed on surfaces.[5−13] For larger molecular systems, STM can resolve submolecular structure resulting either from nuclear positions or from the shape of electron orbitals.[14−18] Information about electronic structure in particular can be acquired from spectroscopic variants of STM, which probe the dependence of the tunneling signal on both the spatial location of the tip and the sign and magnitude of the bias voltage between the tip and sample. In this fashion, experiments can

Received: September 23, 2011
Published: December 16, 2011

   dx.doi.org/10.1021/ja208981y | *J. Am. Chem.Soc.* 2012, 134, 1710−1714

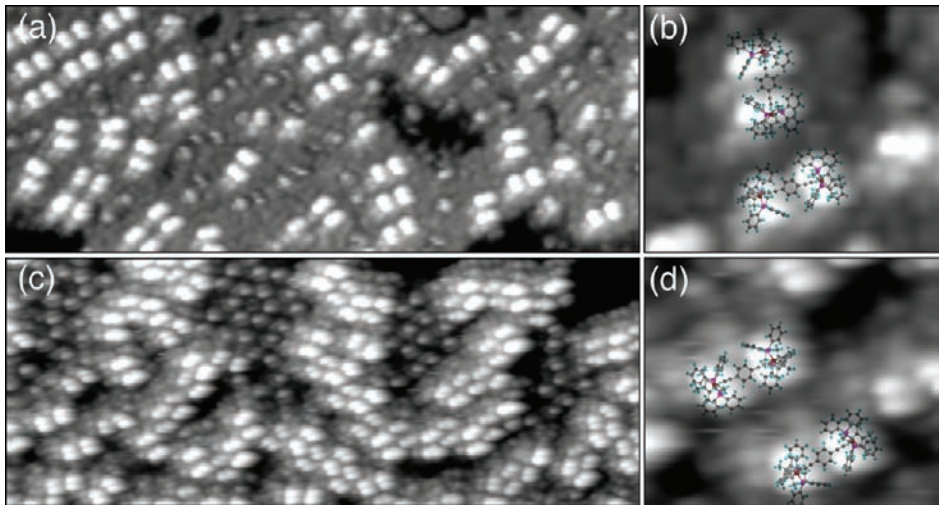

Figure 2. (a) 335 Å × 130 Å, Neutral *para*-Fe2 and THF on Au(111) with a bias voltage of −1.0 V and a tunneling current of 5 pA. (b) 54 Å × 45 Å, Ball-stick model of *para*-Fe2 overlaid on enlarged portion of (a). (c) 335 Å × 130 Å, Mixture of neutral *para*-Fe2 and mixed-valence *para*-Fe2 with PF_6^- counterion, ferrocene, and THF on Au(111) with a bias voltage of −1.0 V and a tunneling current of 5 pA. (d) 54 Å × 45 Å, Ball-stick model of *para*-Fe2 overlaid on enlarged portion of (c).

probe the spatial extent and energy of occupied and unoccupied molecular orbitals.[7−9,19]

Neutral and mixed-valence *meta*-Fe2 and *para*-Fe2 were studied by STM at 77 K after pulse deposition onto gold surfaces. Commercial Au(111)-on-mica substrates were used after two rounds of argon-ion sputtering (15 min with 20 mA ion current) and annealing (30 min at 673 K). Solution concentrations of 1.5 mM in THF were prepared in an argon-purged glovebox; mixed-valence species were created through oxidation with a 1:1 ratio of *para*-Fe2 to ferrocenium hexafluorophosphate (97%, Sigma-Aldrich). A pulsed solenoid valve (Parker Instrumentation 9-series, 0.5 mm nozzle diameter, IOTA One driver) was used to deposit a small amount of solution onto the substrate, and the solvent was allowed to evaporate without further surface annealing.[20−26] STM images were acquired at 77 K with a low-temperature scanning tunneling microscope (LT-STM, Omicron Nano-Technology), and data were minimally processed to remove noise.[27]

Previous studies on *meta*-Fe2 in its mixed-valence state have shown that the electron density is localized to the Fe(II) metal center and the STM images show an asymmetrical, dim-bright, double-dot feature.[28] This is similar to the charge-localization behavior observed in infrared spectroscopy, Mössbauer spectroscopy, electron spin resonance, and UV−visible spectroscopy measurements made of *meta*-Fe2 in solution by Lapinte and co-workers.[2] In contrast, mixed-valence *para*-Fe2 delocalizes charge over the molecule when in solution.[29] The difference in properties is attributed to geometric restrictions on the π-electron system, which allows strong coupling between π orbitals in the C−C triple bonds only with an even number of intermediary carbons. This is a through-bond (as opposed to through-space) model of electronic coupling that suggests that *ortho*- and *para*-substituted benzene rings will produce substantially lower barriers to electron tunneling than *meta*-substituted molecules. The STM images presented in Figure 2 show that both neutral (Figure 2a) and a mixture of neutral and mixed-valence (Figure 2c) *para*-Fe2 are imaged as bright features with complete bilateral symmetry. In order to control for experimental variables (in particular, for variations in the structure of the STM tip), we prepared a 1:1 mixture of neutral and mixed-valence *para*-Fe2. Samples were then prepared and imaged, allowing for side-by-side comparison between the two species under near-identical experimental conditions. STM images were acquired at both positive and negative tip−sample bias voltages, and the resulting images are shown in Figure 3.

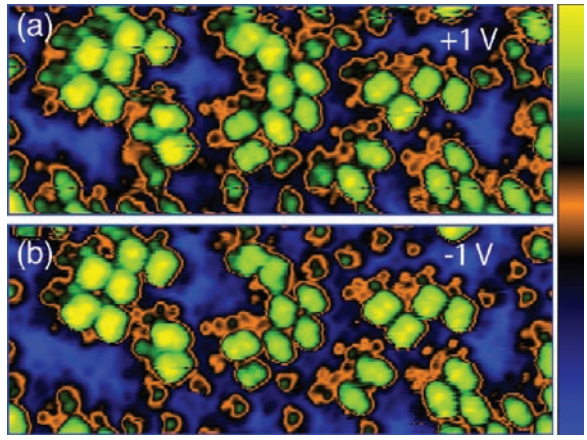

Figure 3. (a) and (b) are 186 Å × 78 Å images of the same area with a bias voltage of +1.0 V/−1.0 V, respectively, and a tunneling current of 10 pA. A mixture of neutral *para*-Fe2, mixed-valence *para*-Fe2 with a PF_6^- counterion, ferrocene, and THF were deposited and imaged on a Au(111) surface. The distribution of electron density for both neutral *para*-Fe2 and mixed-valence *para*-Fe2 remains symmetrical under varying bias voltages.

The symmetric features in Figure 3 match the symmetric features shown in Figure 2. This indicates electron density symmetrically distributed between the two metal centers, in accordance with ensemble measurements of solvated molecules.[4]

In a similar experiment, we prepared a 1:1 mixture of *meta*-Fe2 and *para*-Fe2, both oxidized to their mixed-valence states. Lapinte and co-workers determined that the first oxidation potential of *meta*-Fe2 is between the first and second oxidation potential of *para*-Fe2 allowing coexistence of mixed-valence

dx.doi.org/10.1021/ja208981y | *J. Am. Chem.Soc.* 2012, 134, 1710−1714

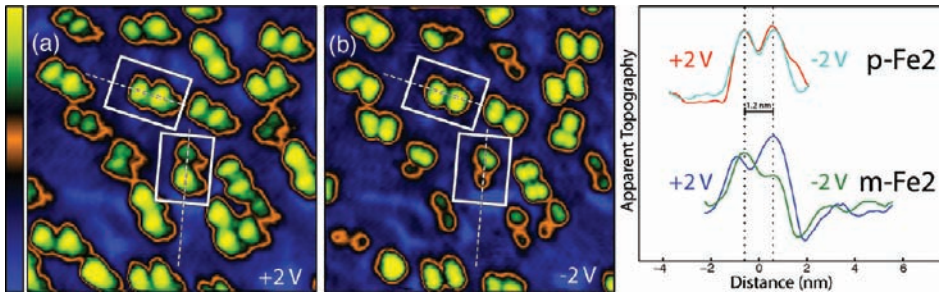

Figure 4. (a) and (b) are 162 Å × 159 Å images of the same area with a bias voltage of +2.0 V/−2.0 V and a tunneling current of 10 pA/100 pA, respectively. The outlined molecules near the top of the figure are *para*-Fe2. The electron density of *para*-Fe2 remains symmetrical under varying bias voltages. The outlined molecules on the lower portion of the figure are *meta*-Fe2. The electron density of *meta*-Fe2 is asymmetrical with the occupied electron orbitals of the Fe(II) creating the brighter lobe in the image taken with a negative bias voltage and the electron-deficient Fe(III) appearing as the brighter lobe in the image taken with a positive bias.

para-Fe2 and mixed-valence *meta*-Fe2.[3] STM images were acquired at both positive and negative tip−sample bias voltages, and the resulting images are shown in Figure 4. A bias voltage of ±2 V was used to ensure tip stability during the experiment. The relatively high bias voltage did not perturb the electronic properties of the molecules, as similar results were achieved during previous experiments with bias voltages of ±0.5 V. All images contain symmetric features that match those in Figures 2 and 3, and which we assume are *para*-Fe2 molecules; asymmetric bright-dim features are assumed to result from *meta*-Fe2, as they are similar to those in images we reported in ref 28. A small selection of molecules in Figure 4 appear as symmetrically bright or dim when imaged with a negative bias and remain symmetrical but switch to dim or bright when imaged with a positive bias. Due to large comproportionation constants, we would only expect a very small amount of neutral or doubly oxidized molecules to be present on the surface.[3] However, our glovebox and balance are not ideal for working with small quantities of Fe2 molecules and it is possible that the stoichiometry of $FcPF_6$ and Fe2 may not have been precisely 1:1, allowing for the presence of some neutral or doubly oxidized *meta*- or *para*-Fe2. Symmetric and asymmetric features are present at equal coverage, within the relatively broad limits imposed by solution preparation.

Switching the polarity of the tip−sample bias allows us to image both filled and empty electron states of the adsorbed molecules. Comparison of the image taken with a positive bias voltage and the image taken with a negative bias voltage from Figures 4 and 3 shows that while symmetric features remain symmetric, asymmetric features flip their asymmetry. This is an observation of a contrast inversion with bias voltage. For a feature whose imaged topography depended on molecular geometry alone, some change in contrast with tunneling conditions is not uncommon, but a reversal of what is imaged as higher and what is lower would not be expected from a purely topographic feature. This reinforces the assignment of the asymmetry as electronic in nature: when filled states are imaged at negative sample bias, the Fe(II) side of *meta*-Fe2 appears brighter than the relatively electron-deficient Fe(III). When empty states are imaged at positive sample bias, the Fe(III) side of the molecule then becomes significantly brighter. The distribution of electron density for *para*-Fe2 remains symmetrical when imaged with both a positive and negative sample bias. A direct comparison of electron distribution in *meta*-Fe2 and *para*-Fe2 is facilitated by the height cross sections in Figure 4.

There are potential caveats in interpreting the results of these experiments. In particular, it is important to consider the possibility that molecules prepared in solution in one oxidation state might change their oxidation state upon adsorption on the surface. A straightforward assessment of the relevant oxidation potentials suggests they should not: the oxidation potential for *para*-Fe2 (−0.315 V vs SCE) is slightly more negative than *meta*-Fe2 (−0.225 V vs SCE), but both are enough below the oxidation potential of Au(111) that we might not expect adsorption induced reduction to be spontaneous for either molecule.[3,30] However, this approach is too simple, as this is one of the key questions motivating this study: the extent to which solution-based oxidation and reduction processes are affected by removal of solvent and adsorption onto a metal surface. The position of the Au(111) Fermi level is certainly affected not only by the adsorption of a polar molecule but also by the partial monolayer of solvent molecules formed. Furthermore, it is unlikely that molecule-surface electron transfer would be driven by the thermodynamics of oxidation and reduction alone, as the absence of solvent means that the ion−counterion complex cannot be readily dissociated.

For *meta*-Fe2, the experimental data clearly show that preparation of different oxidation states in solution results in different adsorbed species. In particular, the contrast between the images of the occupied and unoccupied orbitals of *meta*-Fe2 indicate that it remains a mixed-valence species on the Au(111) surface. Close examination of images of samples with mixtures of neutral and mixed-valence *para*-Fe2 (Figures 2c and 3) shows two slightly different but distinct types of molecular features, in support of there being two chemically distinct species on the surface for *para*-Fe2 as well. However, these differences are quite small and could also result from disparate adsorption geometries. All of these factors considered, *meta*-Fe2 and *para*-Fe2 are present in the same environment: a Au(111) surface, THF, ferrocene, and a PF_6^- counterion. While still considering the above discussion, then, the simplest explanation is that the contrast in charge localization is due to the difference in connectivity of the Cp*Fe(dppe) moiety to the central phenyl ring and not due to the influence of the molecular environment. More complex explanations are also plausible: for example, the difference in molecular structure between *meta*-Fe2 and *para*-Fe2 will lead to corresponding differences in the adsorption geometry on the surface, and properties highly sensitive to this geometry might be affected as a consequence. To the extent that a surface-mediated interaction helps couple the two metal centers, we must consider the possibility that delocalization in the *para*-Fe2

dx.doi.org/10.1021/ja208981y | *J. Am. Chem.Soc.* 2012, 134, 1710−1714

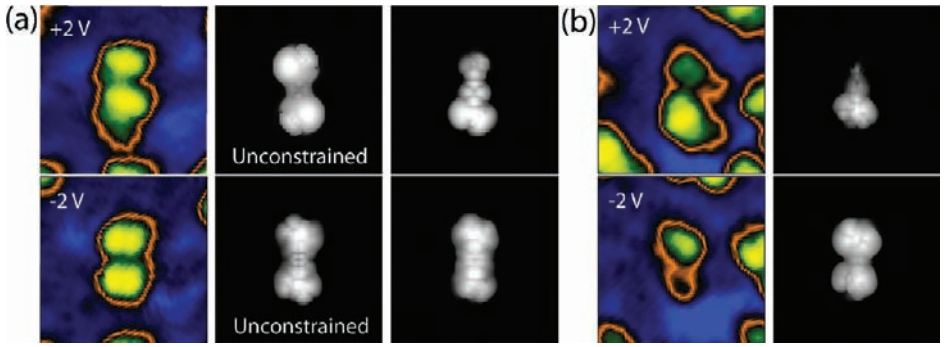

Figure 5. Comparison of simulated and experimental STM images under opposite biases. Simulated images are demonstrated in black and white. Experimental images are shown in color. (a) Images of *para*-Fe2 mixed-valence complexes; best agreement is between experiment and unconstrained, charge-delocalized DFT calculation. (b) Images of *meta*-Fe2 mixed-valence complexes; best agreement is between experiment and charge-localized CDFT calculation.

compound occurs via through-metal (as opposed to through-bond) coupling.

We have carried out electronic-structure calculations for *para*-Fe2 and *meta*-Fe2 in both neutral and mixed-valence states. Density functional theory (DFT) is appropriate for describing both *para*-Fe2 and neutral *meta*-Fe2; however, calculations for the mixed-valence *meta*-Fe2 use constrained DFT (CDFT), which was developed to overcome the overestimation of charge delocalization suffered by traditional DFT methods.[31−34] All calculations are carried out using the NWCHEM software package.[35] The B3LYP exchange-correlation potential is employed in the DFT calculation. 6-311G** basis sets are used for C, H, and P atoms, and the ECP basis LANL2TZ(f) is used for Fe atoms. To reduce computational effort, we replace the bidentate dppe ligand with pairs of hydrogen-terminated phosphorus atoms, $(PH_3)_2$, as we did previously.[28] Nuclear geometries were then optimized, followed by computation of electron densities for both empty and filled electronic states.

Simulated STM images were computed first by modeling the predicted tunneling current as a function of tip position, and experiment is matched by plotting a surface that keeps this current constant. The Tersoff and Hamann approach would set the tunneling current for any given tip position as the local density of electronic states at that position.[36−38] This is particularly ill-suited to systems such as ours where the molecule is large, and where there are significant variations in electron density as a function of all three directions in space.[39] The Bardeen approach, which models the tunneling probability through calculation of the overlap of separate tip and sample wave functions, is far more suitable but requires significantly more involved calculations.[37,38,40] To produce simulated tunneling currents, we approximate the effects of tip−sample wave function overlap by considering not just the local density of states at the tip position, but an integral of the state density along the tunneling axis, weighted exponentially by proximity to the tip. In the limit of rapid exponential decay this reduces to the Tersoff−Hamann approach, but away from that limit this includes the effect of high-state-density regions even if the tip is some distance away. To produce simulated STM images, the surface was modeled as a featureless and constant density of states at one edge of the box used in calculations; the tunneling current due to the surface alone is thus an exponentially decaying function of distance, which is the physically reasonable result.

Simulated STM images are surfaces of constant calculated current, as calculated above. Because the electronic-structure calculations do not include the dppe ligands or the Au surface, we do not expect quantitative agreement with experiment. Instead, we use them in a limited role: as a measure of the extent to which charge localization in a mixed-valence molecule will appear in an STM image. Simulated and experimental images are shown side-by-side in Figure 5. Figure 5a presents images of *para*-Fe2 mixed-valence species. Under both positive and negative gap voltage, the *para*-Fe2 mixed-valence complex exhibits a symmetric two-dot structure, which demonstrates that the mobile charge is delocalized between two Cp*Fe(dppe) moieties. Any asymmetry in electron distribution would be apparent in these data, as a CDFT calculation that localizes charge on one side of the *para*-Fe2 molecule produces simulated images that do not match experiment. For comparison, DFT calculations of neutral *para*-Fe2 (shown immediately to the right of the experimental images) show symmetrical distribution of electron density between the two metal centers and predict correspondingly symmetric images, providing a good match to the experimental images of both neutral and mixed-valence *para*-Fe2. The charge delocalization indicated in both simulated and experimental STM images is in agreement with the fact that the *para*-Fe2 cation is a borderline type II/type III mixed-valence complex according to the Robin−Day classification.[4]

Figure 5b shows images of *meta*-Fe2 mixed-valence complexes. In these images, the mobile charge is localized on one Cp*Fe(dppe) moiety, resulting in a brighter-dimer two-dot structure associated with each molecule, as described above and reported in our previous study.[28] The inversion of this contrast (brighter-dimmer to dimmer-brighter) that accompanies a change in tip−sample bias is matched in the shapes of the molecular orbitals calculated by CDFT, though this contrast is much more pronounced for the calculations at positive bias voltages. Although the CDFT calculations do not include the full Cp*Fe(dppe) ligand structure, the agreement in kind and magnitude between experiment and simulation provides additional confirmation that the asymmetry of mixed-valence *meta*-Fe2 results from asymmetry in the electronic structure of the molecule.

The observation of charge localization in single, surface-adsorbed *meta*-Fe2 molecules alongside charge delocalization in *para*-Fe2 molecules allows for a number of strong conclusions to be drawn. First, intramolecular charge transfer in these molecules occurs through the extended alkyne−benzene−

dx.doi.org/10.1021/ja208981y | *J. Am. Chem.Soc.* 2012, 134, 1710−1714

alkyne system (or potentially via coupling through the substrate), as opposed to electron tunneling through space; this is reinforced by the fact that the Fe−Fe distance is larger in *para*-Fe2, and yet electronic coupling is stronger. Second, localization of charge in these mixed-valence molecules is not induced solely by polarization of nearby solvent, as qualitatively similar localization is observed for solvated molecules and surface-adsorbed molecules in vacuum. Third, in the surface-adsorbed system, neither the polarizability of the metal substrate nor the presence of the PF_6^- counterion is responsible for charge localization in *meta*-Fe2, as both of these are present in similar fashion for *para*-Fe2 where localization is not observed.

AUTHOR INFORMATION

Corresponding Author

skandel@nd.edu

ACKNOWLEDGMENTS

This work was supported by the National Science Foundation under NSF CHE-0848415 and NSF CHE-1124762.

REFERENCES

(1) Weyland, T.; Ledoux, I.; Brasselet, S.; Zyss, J.; Lapinte, C. *Organometallics* **2000**, *19*, 5235.
(2) Weyland, T.; Costuas, K.; Toupet, L.; Halet, J. F.; Lapinte, C. *Organometallics* **2000**, *19*, 4228.
(3) Weyland, T.; Lapinte, C.; Frapper, G.; Calhorda, M.; Halet, J.; Toupet, L. *Organometallics* **1997**, *16*, 2024.
(4) Le Narvor, N.; Lapinte, C. *Organometallics* **1995**, *14*, 634.
(5) Kleiner-Shuhler, L.; Brittain, R.; Johnston, M. R.; Hipps, K. W. *J. Phys. Chem. B* **2008**, *112*, 14907.
(6) Takami, T.; Mazur, U.; Hipps, K. W. *J. Phys. Chem. C* **2009**, *113*, 17479.
(7) Grobis, M.; Lu, X.; Crommie, M. F. *Phys. Rev. B* **2002**, *66*, 161408.
(8) Grobis, M.; Yamachika, R.; Wachowiak, A.; Lu, X. H.; Crommie, M. F. *Phys. Rev. B* **2009**, *80*, 073410.
(9) Wang, Y. Y.; Yamachika, R.; Wachowiak, A.; Grobis, M.; Khoo, K. H.; Lee, D. H.; Louie, S. G.; Crommie, M. F. *Phys. Rev. Lett.* **2007**, *99*, 086402.
(10) Wang, W. H.; Shi, X. Q.; Lin, C. S.; Zhang, R. Q.; Minot, C.; Van Hove, M. A.; Hong, Y. N.; Tang, B. Z.; Lin, N. *Phys. Rev. Lett.* **2010**, *105*, 126801.
(11) Wei, Z. Q.; Guo, S.; Kandel, S. A. *J. Phys. Chem. B* **2006**, *110*, 21846.
(12) Guo, S.; Kandel, S. A. *J. Chem. Phys. Lett.* **2010**, *1*, 420.
(13) Pascual, J. I.; Jackiw, J. J.; Song, Z.; Weiss, P. S.; Conrad, H.; Rust, H. P. *Surf. Sci.* **2002**, *502*, 1.
(14) Treier, M.; Ruffieux, P.; Fasel, R.; Nolting, F.; Yang, S. F.; Dunsch, L.; Greber, T. *Phys. Rev. B* **2009**, *80*, 081403.
(15) Kim, H.; Son, W. J.; Jang, W. J.; Yoon, J. K.; Han, S.; Kahng, S. J. *Phys. Rev. B* **2009**, *80*, 245402.
(16) Hou, J. G.; Yang, J. L.; Wang, H. Q.; Li, Q. X.; Zeng, C. G.; Yuan, L. F.; Wang, B.; Chen, D. M.; Zhu, Q. S. *Nature* **2001**, *409*, 304.
(17) Qiu, X. H.; Nazin, G. V.; Ho, W. *Science* **2003**, *299*, 542.
(18) Weiss, P. S.; Eigler, D. M. *Phys. Rev. Lett.* **1993**, *71*, 3139.
(19) Haider, M. B.; Pitters, J. L.; DiLabio, G. A.; Livadaru, L.; Mutus, J. Y.; Wolkow, R. A. *Phys. Rev. Lett.* **2009**, *102*, 046805.
(20) Guo, S.; Kandel, S. A. *J. Chem. Phys.* **2008**, *128*, 014702.
(21) Kanno, T.; Tanaka, H.; Nakamura, T.; Tabata, H.; Kawai, T. *Jpn. J. Appl. Phys.* **1999**, *38*, L606.
(22) Bernard, R.; Huc, V.; Reiss, P.; Chandezon, F.; Jegou, P.; Palacin, S.; Dujardin, G.; Comtet, G. *J. Phys.: Condens. Matter* **2004**, *16*, 7565.
(23) Grill, L.; Stass, I.; Rieder, K. H.; Moresco, F. *Surf. Sci.* **2006**, *600*, L143.
(24) Shirai, Y.; Osgood, A. J.; Zhao, Y. M.; Kelly, K. F.; Tour, J. M. *Nano Lett.* **2005**, *5*, 2330.
(25) Terada, Y.; Choi, B. K.; Heike, S.; Fujimori, M.; Hashizume, T. *Nano Lett.* **2003**, *3*, 527.
(26) Terada, Y.; Choi, B. K.; Heike, S.; Fujimori, M.; Hashizume, T. *J. Appl. Phys.* **2003**, *93*, 10014.
(27) Fogarty, D. P.; Deering, A. L.; Guo, S.; Wei, Z. Q.; Kautz, N. A.; Kandel, S. A. *Rev. Sci. Instrum.* **2006**, *77*, 126104.
(28) Lu, Y. H.; Quardokus, R.; Lent, C. S.; Justaud, F.; Lapinte, C.; Kandel, S. A. *J. Am. Chem. Soc.* **2010**, *132*, 13519.
(29) Ghazala, S. I.; Paul, F.; Toupet, L.; Roisnel, T.; Hapiot, P.; Lapinte, C. *J. Am. Chem. Soc.* **2006**, *128*, 2463.
(30) Scudiero, L.; Barlow, D.; Mazur, U.; Hipps, K. *J. Am. Chem. Soc.* **2001**, *123*, 4073.
(31) Wu, Q.; Van Voorhis, T. *J. Chem. Theory Comput.* **2006**, *2*, 765.
(32) Wu, Q.; Van Voorhis, T. *J. Phys. Chem. A* **2006**, *110*, 9212.
(33) Wu, Q.; Van Voorhis, T. *Phys. Rev. A* **2005**, *72*, 024502.
(34) Dederichs, P. H.; Blugel, S.; Zeller, R.; Akai, H. *Phys. Rev. Lett.* **1984**, *53*, 2512.
(35) Valiev, M.; Bylaska, E. J.; Govind, N.; Kowalski, K.; Straatsma, T. P.; Van Dam, H. J. J.; Wang, D.; Nieplocha, J.; Apra, E.; Windus, T. L.; de Jong, W. *Comput. Phys. Commun.* **2010**, *181*, 1477.
(36) Tersoff, J.; Hamann, D. R. *Phys. Rev. B* **1985**, *31*, 805.
(37) Blanco, F. F.; R. Pérez, J. M. *Prog. Surf. Sci.* **2006**, *81*, 403.
(38) Hayes, R. L.; Tuckerman, M. E. *J. Phys. Chem. C* **2010**, *114*, 15102.
(39) Probst, O. M. *Am. J. Phys.* **2002**, *70*, 1110.
(40) Bardeen, J. *Phys. Rev. Lett.* **1961**, *6*, 57.